

# Fast multi-scale edge-detection in medical ultrasound signals.

Preben Gråberg Nes

Department of Mathematics, Norwegian University of Science of Technology

N-7491 Trondheim, Norway

e-mail:preben.nes@math.ntnu.no

## Abstract

In this article we suggest a fast multi-scale edge-detection scheme for medical ultrasound signals. The edge-detector is based on well-known properties of the continuous wavelet transform. To achieve both good localization of edges *and* detect only significant edges, we study the maxima-lines of the wavelet transform. One can obtain the maxima-lines between two scales by computing the wavelet transform at several intermediate scales. To reduce computational effort and time we suggest a time-scale filtering procedure which uses only few scales to connect modulus-maxima across time-scale plane. The design of this procedure is based on a study of maxima-lines corresponding to edges typical for medical ultrasound signals. This study allows us to construct an algorithm for medical ultrasound signals which meets the demand for speed, but not on expense of reliability.

The edge-detection algorithm has been applied to a large class of medical ultrasound signals including tumour-, liver- and artery-images. Our results show that the proposed algorithm effectively detects major features in such signals, including edges with low contrast.

## 1 Introduction

Recent advances within medical research calls for new techniques to improve the quality of medical ultrasound signals. Ultrasound is versatile and non-invasive compared to many other medical visualization-systems. Unfortunately ultrasound signals are often heavily contaminated with speckle-noise. In addition, edges in such signals often have low contrast. This makes medical ultrasound signals difficult to interpret and analyze. Improving the quality of such signals is therefore desirable.

In this article we study a fast wavelet-based edge-detector scheme for medical ultrasound signals. This scheme is based on properties of the continuous wavelet transform. We refer to [1] and [2, Ch. 6] for an introduction to the wavelet transform as well as its application in edge-detection. The continuous wavelet transform can be used to study local structures - such as edges - at different scales in a signal. In particular, if the wavelet is given by the 1st derivative (1-D) or gradient (2-D) of the Gaussian-function, the local extrema (modulus-maxima) of the wavelet transform at a scale correspond to edge-points in the signal.

In order to explain the idea behind our investigation we will give a brief survey of the now classic Canny edge-detector [3]. The Canny edge-detector computes the wavelet transform of a signal at a single scale. If the modulus of the wavelet transform at a modulus-maximum is larger than a threshold-value its spatial location represents an edge. At a fine scale the Canny edge-detector provides fine details, but is sensitive to noise. At a coarse scale one can detect low-contrast edges, but the positional accuracy of a modulus-maximum is poor compared to the location of the edge.

At each scale the wavelet transform yields a different description of the edges in the signal. It is clear that for a noisy signal - such as a medical ultrasound signal - there is no single scale which provides a categorically correct representation of the edges. To deal with this ambiguity we - as many others e.g. [4, 5, 6, 7, 8, 9] - suggest to use the wavelet transform at several scales. The idea is to study modulus-maxima at coarse scales to detect the edges, and use a fine scale to localize them.

The main purpose of this article is to address two issues which frequently occur when using multi-scale wavelet transform to detect edges. These are;

1. Which modulus-maxima at different scales correspond to the same edge in the underlying signal, and
2. how can one effectively decide which modulus-maxima correspond to the same edge.

As the scale decreases each modulus-maximum belongs to a curve (maxima-line) in the time-scale plane. As  $s \rightarrow 0$  each maxima-line propagates towards an edge in the signal. The maxima-lines provide a natural identification of which modulus-maxima corresponds to the same edge in the signal.

To decide which modulus-maxima belong to the same maxima-line one can compute the wavelet transform at several close scales and gradually trace the modulus-maxima towards fine scales [4, 5]. However, the wavelet transform computed at two close scales carries almost the same information, and do not contribute with new information with regards to the edge-detector scheme studied in this article. Computing the wavelet transform at several scales will therefore yield redundancy, as well as making the procedure computationally expensive.

Our aim is to decide which modulus-maxima belong to the same maxima-line by computing the wavelet transform at only a few 'different' scales. To achieve this it is essential to understand the behavior of the maxima-lines in the time-scale plane. This depends on several factors, such as the intensity and mutual position of the edges. In general the ambiguity introduced by using multiple scales is inescapable. The goal is not to eliminate the ambiguity, but rather manage it and reduce it where possible.

For this purpose we study typical maxima-lines corresponding to medical ultrasound signals. It happens that local intensity-changes in medical ultrasound signals often can be approximated by a set of model-edges. In this article we refer to these as patterns. In particular, the maxima-lines of each pattern have their special behavior in the time-scale plane.

To the best of our knowledge the idea of using model-edges to study properties of the wavelet transform in the time-scale plane is due to [10] who created an 'elementary' set of model-edges. Since then this idea has been used by a number of researchers e.g. [11] and more recently [12].

We propose a new time-scale filtering procedure for medical ultrasound signals. This procedure accommodates the time-scale behavior of both the maxima-lines and the wavelet transform corresponding to the set of patterns. The procedure uses a decision-function which analyzes a decay- and a distance-criterion to decide which modulus-maxima belong to the same maxima-line. The procedure is constructed to decide this by computing the wavelet transform at only a sparse set of scales.

The set of patterns serves as test signals for the time-scale filtering procedure. By analyzing the accuracy of the decision-function on the maxima-lines corresponding to each pattern we study the reliability of the procedure. We complement this with a statistical study on medical ultrasound signals.

We also study an edge-detector scheme for medical ultrasound images which is based on the time-scale filtering procedure. The edge-detector uses a perceptual criteria similar to [6] to find the

significant edges in an image. This method has shown promising results for detecting and localizing (low-contrast) edges in medical signals.

Several have suggested edge-detectors based on the multi-scale wavelet transform. We refer to [13] and references therein for a general exposition of edge-detectors. In [14, 15, 12] edges are characterized by estimating the decay of the wavelet transform along each maxima-line. In [6, 9] they use multi-scale wavelet coefficients to detect and localize significant edges, and in [16, 17] the authors suggest a procedure using automatic scale selection. Statistical methods have been used in [18], and in [7] a method based on the multi-scale Edge-flow vector field have been proposed.

The article is organized as follows. In the next section we provide a brief reminder of the wavelet transform and its use to detect edges. We also discuss general properties of maxima-lines related to edge-detection. In Sect.3 we propose and study a time-scale filtering procedure for medical ultrasound signals. We conclude Sect.3 with a discussion of a space-scale filtering procedure for images. This construction is based on our analysis of the 1-D time-scale filtering procedure. In Sect.4 we present the edge-detection algorithm. In the final part of the note we present experimental results of both time-scale filtering procedure and edge-detection algorithm. These results are based on a study of both phantom and actual medical ultrasound images.

## 2 Wavelet transform.

### 2.1 Wavelet transform.

We consider the following well-known smoothing-function and wavelet;

$$\begin{aligned}\theta(t) &= \pi^{-1/4} e^{-\frac{t^2}{2}}, \\ \psi(t) &= -\sqrt{2} \theta'(t) = \sqrt{2} \pi^{-1/4} t e^{-\frac{t^2}{2}}.\end{aligned}$$

The wavelet transform is defined as e.g. in [2];

$$Wf(u, s) = \int_{\mathbb{R}} f(t) \frac{1}{\sqrt{s}} \psi\left(\frac{t-u}{s}\right) dt.$$

The candidate edges of  $f$  correspond to the points  $(u, s)$  in the time-scale plane where  $|Wf(\cdot, s)|$  has a local maximum. These points are referred to as modulus-maxima, in what follows abbreviated mod-max. The set of mod-max of  $Wf(u, s)$  at a scale  $s > 0$  will be denoted  $\mathcal{M}f(s)$ ;

$$\mathcal{M}f(s) = \{u : u \text{ is a local-maximum of } |Wf(\cdot, s)|\}.$$

For 2-D signals (images) J. Canny introduced an edge-detector in [3]. This was later formulated in wavelet terminology by e.g. [15]. The smoothing function and (directional) wavelets are given by;

$$\begin{aligned}\theta(x, y) &= \theta(x)\theta(y), \\ \psi^x(x, y) &= \psi(x)\theta(y), \quad \psi^y(x, y) = \theta(x)\psi(y),\end{aligned}$$

where  $\theta(\cdot)$  and  $\psi(\cdot)$  are defined as above. Given a function  $f$  in two variables, let  $f_s(x, y) = s^{-1}f(s^{-1}x, s^{-1}y)$ . The 2-D wavelet transform is defined as;

$$Wf((u, v), s) = \begin{pmatrix} W^x f((u, v), s) \\ W^y f((u, v), s) \end{pmatrix} = s \nabla (f * \theta_s)(x, y).$$

The vector  $Wf$  is the direction of maximal change of the smoothed image  $f * \theta_s$ . Candidate edges are the points  $((u, v), s)$  in the space-scale plane where  $|Wf((u, v), s)|$  has a local maximum in

the direction of maximal change. The set of mod-max at scale  $s$  will in what follows be denoted  $\mathcal{M}f(s)$ ;

$$\mathcal{M}f(s) = \{(u, v) : (u, v) \text{ is a directional local maximum of } Wf((\cdot, \cdot), s)\}.$$

## 2.2 Maxima-lines.

With respect to the wavelet considered in this article it is well-known that every mod-max of  $\mathcal{M}f(s)$  belongs to some curve

$$\ell = \{(u, s) : u = \ell_a(s), a \in A\},$$

where  $A$  is some index-set. These curves are called maxima-lines. For wavelets equal a derivative of the Gaussian-function every maxima-line  $\ell_a(s)$  propagates towards finer scales [2, page 178], see fig.1 for an example. In particular, if no maxima-lines propagate towards a point in an interval it

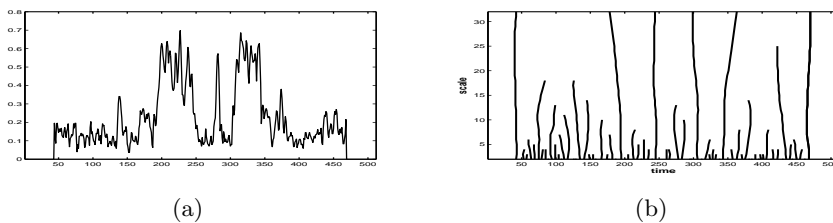


Figure 1: (a) A 1-D ultrasound signal. (b) The maxima-lines of  $Wf(u, s)$ .

contains no edges [2, Th. 6.5].

It will be assumed that a mod-max at a scale corresponds to only one mod-max at any finer scales. In theory a maxima-line may bifurcate, but the probability of bifurcating in real signals is negligible.

To illustrate this we consider the function  $f(t) = \rho(t) + A\rho(t-1)$  where  $A > 0$  and  $\rho(t)$  denotes the Heaviside-function (we remind the definition of  $\rho(t)$  in Sect.3.2). The mod-max of  $Wf(u, s)$  are found by solving

$$te^{-\frac{t^2}{2s^2}} + A(t-1)e^{-\frac{(t-1)^2}{2s^2}} = 0 \Leftrightarrow \ln A + \ln \frac{1-t}{t} = \frac{1}{s^2} \left( \frac{1}{2} - t \right).$$

There exists a  $s^* > 0$  (see (3)) such that this equation has one and only one solution for every  $s > s^*$  and three solutions (two modulus-maxima and one local minimum) for  $s < s^*$ . It is clear that the solution curves (maxima-lines) bifurcate if and only if  $\ln A = 0$  i.e.  $A = 1$ . For all other values of  $A$  the maxima-lines do not bifurcate. Our study of maxima-lines in medical ultrasound signals indicates that bifurcations are rare in such signals.

We will also assume that two mod-max on the same maxima-line correspond to the same underlying phenomenon in the signal, and that the accuracy of the localization of the mod-max increases as  $s$  decreases. These assumptions corresponds to the classical identity- and localization-assumption of Witkin [5].

## 3 Space-scale filtering.

The main purpose of this article is to study how one can connect mod-max between two (perhaps rather distinct) scales. Let  $\ell_a, a \in A$  be the maxima-lines of  $Wf(u, s)$ , and

$$\mathcal{M}f(s_i) = \{\ell_a(s_i) : a \in A\}, \quad i = 1, 2$$

be the mod-max at two scales. If  $s_2 > s_1$  the number of elements in  $\mathcal{M}f(s_2)$  is less or equal the number of elements in  $\mathcal{M}f(s_1)$  since new maxima-lines may appear between  $s_2$  and  $s_1$ . The question is how one can decide which mod-max of  $\mathcal{M}f(s_1)$  belong to the same maxima-line as a mod-max of  $\mathcal{M}f(s_2)$ , and which belong to a maxima-line which appears between  $s_2$  and  $s_1$ .

At fine scales one can decide which mod-max belong to the same maxima-line by considering their spatial distance. At coarse scales one can consider the logarithmic-decay of the wavelet transform. In addition the sign of the wavelet transform along a maxima-line can not change.

In the next section we suggest a time-scale filtering procedure for medical ultrasound signals. This procedure is based on a decision-function  $P(\cdot, \cdot)$  which analyzes *both* a distance- *and* a decay-criterion to decide which mod-max belong to the same maxima-line. We design the function to favor decay at coarse scales and distance at fine scales. In Sect.3.2 we introduce a set of model-edges, called patterns, which serves as test-signals for the decision-function. These patterns model local intensity-changes in medical ultrasound signals. In Sect. 3.3 we study the reliability of the time-scale filtering procedure with respect to each pattern and their respective maxima-lines.

### 3.1 Decision-function and time-scale filtering procedure.

Let  $s_2, s_1$  be two scales  $s_2 > s_1$ , and let  $(n, s_2)$  and  $(m, s_1)$  be two mod-max. We define the decision-function corresponding to scales  $s_2$  and  $s_1$  as;

$$P(n, m) = \Delta(n, m)D(n, m)\text{Sign}(n, m), \quad (1)$$

where;

$$\begin{aligned} \Delta(n, m) &= \exp(-|n - m|s_1^{-\alpha}), \\ D(n, m) &= \exp\left(-\left|\ln \frac{|Wf(n, s_2)|}{|Wf(m, s_1)|} \ln^{-1} \frac{s_2}{s_1} - \frac{1}{2}\right|s_1^\alpha\right), \\ \text{Sign}(n, m) &= \begin{cases} 1 & \text{if } \text{sign}\left(\frac{Wf(n, s_2)}{Wf(m, s_1)}\right) = 1 \\ 0 & \text{otherwise.} \end{cases} \end{aligned}$$

The essence of the procedure is to connect mod-max which maximize the decision-function  $P(\cdot, \cdot)$ . For instance, if  $(n, s_2)$  and  $(m, s_1)$  *both* belong to the same maxima-line  $\ell_a$  say, then we want  $P(n, m) > P(n, u)$  for all  $u \in \mathcal{M}f(s_1), u \neq m$ . The control-parameter  $\alpha$  in the expressions of  $\Delta$  and  $D$  controls the mutual weighting between the distance- ( $\Delta$ ) and decay-criterion ( $D$ ). A negative  $\alpha$  favors the decay-criterion, while a positive favors distance. By studying the procedure for various choices of  $\alpha$  we find a weighting between distance and decay suitable for our type of signals.

In the following sections we will analyze the decision function  $P(\cdot, \cdot)$  and the corresponding time-scale filtering procedure. This analysis is based on a set of model-edges which model local intensity changes in ultrasound signals.

### 3.2 Patterns

To investigate whether the suggested procedure successfully connects mod-max between two scales we have studied a collection of model-edges, called *patterns*. These patterns - six in total - model typical transitions between tissues in medical ultrasound signals, fig.2.

Let  $\rho_x$  denote the translated Heaviside-function;

$$\rho_x(t) = \begin{cases} 1 & t \geq x \\ 0 & t < x. \end{cases}$$

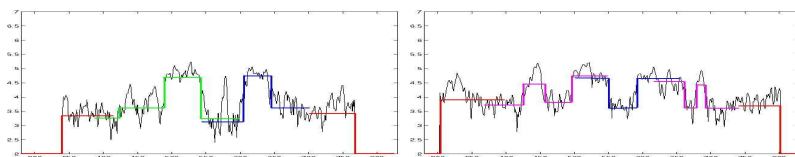


Figure 2: Illustration of how one can locally model edges in medical ultrasound signals with the patterns from Sect.3.2.

The patterns can be modeled as;

$$\begin{aligned}
 \text{Pattern 1 : } & f(t) = \rho_0(t), \\
 \text{Pattern 2 : } & f(t) = \rho_0(t) - B\rho_\beta(t), & B, \beta > 0, \\
 \text{Pattern 3 : } & f(t) = \rho_0(t) + A\rho_1(t), & A > 1, \\
 \text{Pattern 4 : } & f(t) = \rho_0(t) + A\rho_1(t) - B\rho_\beta(t), & A, \beta > 1, B^* > B > 0, \\
 \text{Pattern 5 : } & f(t) = \rho_0(t) + A\rho_1(t) - B\rho_\beta(t), & \beta > 1, B > 0, A^* > A > 0, \\
 \text{Pattern 6 : } & f(t) = \rho_0(t) - B\rho_\beta(t) + A\rho_1(t), & 1 > \beta > 0, A, B > 0.
 \end{aligned}$$

The six patterns each model a particular type of edge. Pattern 1 models an isolated step-edge, that is, if the intensity at the boundary of the object changes at a single jump. Pattern 2 models a thin object or an impulse, while Pattern 3 models a boundary where the intensity changes at two isolated jumps. Pattern 4 and pattern 5 model an object with boundary similar to Pattern 3, but where the intensity decreases shortly after the initial intensity-changes. This occurs for instance if there is a 'void' within the object. If the object has a 'hole' near the boundary one can model this with Pattern 6.

Pattern 4 and pattern 5 differ by the time-scale behavior of the maxima-lines, fig.3(h,j). Given  $A, \beta$  (or  $B, \beta$ ) the point of transformation between the patterns are given by  $B^*$  (or  $A^*$ ).  $B^*$  or  $A^*$  can be found by solving;

$$\begin{cases} \frac{\partial Wf(u,s)}{\partial u} = 0 \\ \frac{\partial^2 Wf(u,s)}{\partial u^2} = 0 \\ \frac{\partial^3 Wf(u,s)}{\partial u^3} = 0. \end{cases} \quad (2)$$

Fig.3 shows typical examples of the patterns and their respective maximal-lines. Every pattern can after a suitable normalization and translation be assumed to have an edge at 0 with intensity 1. Pattern 3-6 have (after rescaling) an additional edge at 1 with (positive) intensity  $A$ , and pattern 2,4-6 have an edge of (negative) intensity  $B$  at  $\beta \neq 0, 1$ . The six patterns have one (pattern 1), two (pattern 2,3) and three (pattern 4-6) maxima-lines, in what follows denoted  $\ell_0$ ,  $\ell_1$  and  $\ell_\beta$ .

In fig.3 the six patterns and characteristic examples of their maxima-lines are displayed. As indicated in fig.3h, one can expect that distance between mod-max is a weak criterion for pattern 4. Rather surprisingly this is also the case for pattern 3. Observe that the maxima-lines of these 'simple' patterns show a complexity similar to those in medical ultrasound signals.

A common factor of pattern 3-6 is that there exists a scale where the maxima-line  $\ell_0$  (pattern 3,4,6),  $\ell_1$  (pattern 5) or  $\ell_\beta$  (pattern 6) first appears. This scale is found by solving the equations;

$$\begin{cases} \frac{\partial Wf(u,s)}{\partial u} = 0 \\ \frac{\partial^2 Wf(u,s)}{\partial u^2} = 0. \end{cases} \quad (3)$$

The unique  $s > 0$  for which (3) has a solution is denoted  $s^*$ . As it happens, the suggested time-scale filtering procedure is often most critical near  $s^*$ .

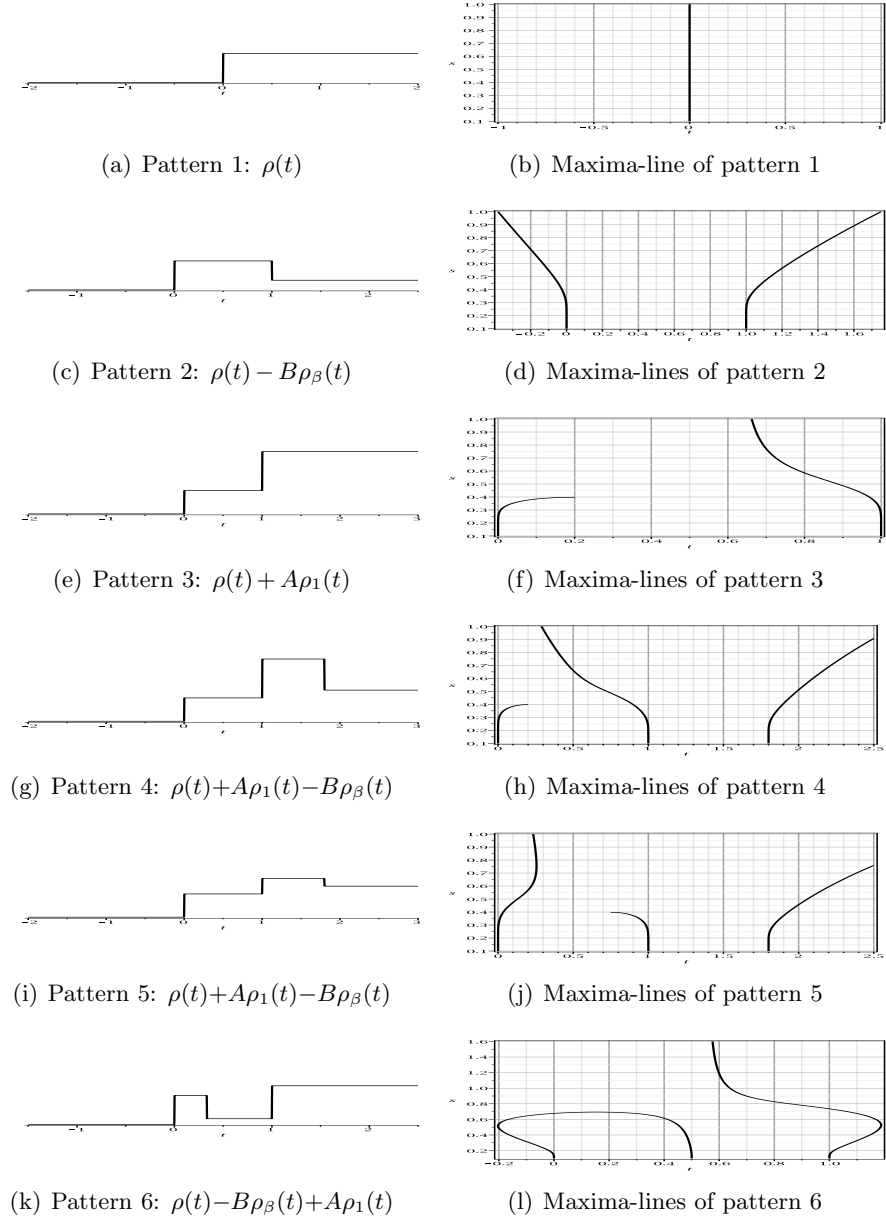


Figure 3: The dictionary of patterns (model edges) used in our analysis. (a) step-edge (c) impulse-edge (e) staircase-edge (g)-(i)-(k) various triplet edges

### 3.3 Evaluation of the time-scale filtering procedure.

The purpose of the forthcoming analysis is to study for which patterns (i.e. for which  $A, B, \beta$ ) the time-scale filtering procedure suggested in Sect.3.1 works. We also study the procedure for different control-parameters  $\alpha$ .

Let as before  $\ell_0$ ,  $\ell_1$  and  $\ell_\beta$  denote the maxima-lines in the patterns from Sect.3.2 and fix two scales  $s_2$  and  $s_1$ . We chose in this study  $s_1 = s_2/2$ , i.e. the scales are dyadic distributed. In what follows let  $P(\cdot, \cdot)$  be the decision-function corresponding to  $s_2$  and  $s_1$  defined in Sect.3.1.

It is straightforward to see that the procedure works for the first two patterns, hence we focus our analysis on patterns 3–6. The decision-function  $P(\cdot, \cdot)$  needs to fulfill one inequality for each maxima-line. Namely; the decision-function connects two mod-max  $\ell_1(s_2)$  and  $\ell_1(s_1)$  from the

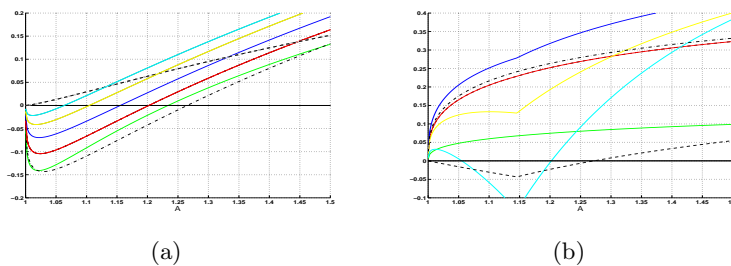


Figure 4: (a) The graph of  $Q_1(A)$  and (b) the graph of  $Q_0(A)$  for  $1 < A < 1.5$ . The cyan, yellow, blue, red, green curves correspond to  $P(n, m)$  defined by (1) with respectively  $\alpha = \{-1/2, 0, 1/2, 1, 3/2\}$  in the expression of  $P$ . The dashed line corresponds to  $P = D$  and dash-dotted line corresponds to  $P = \Delta$ .

maxima-line  $\ell_1$  if;

$$P(\ell_1(s_2), \ell_1(s_1)) - P(\ell_1(s_2), \ell_j(s_1)) > 0 \quad \text{for } j = 0, \beta. \quad (4)$$

Similarly the mod-max  $\ell_0(s_2)$  and  $\ell_0(s_1)$  are connected if;

$$P(\ell_0(s_2), \ell_0(s_1)) - P(\ell_0(s_2), \ell_j(s_1)) > 0 \quad \text{for } j = 1, \beta. \quad (5)$$

Note that for pattern 3 the inequalities (4) and (5) have to hold only for  $j=0$  and  $j=1$  respectively since  $\ell_\beta$  does not exist. Finally, for pattern 4-6 the suggested procedure connects two mod-max from the maxima-line  $\ell_\beta$  if;

$$P(\ell_\beta(s_2), \ell_\beta(s_1)) - P(\ell_\beta(s_2), \ell_j(s_1)) > 0 \quad \text{for } j = 0, 1. \quad (6)$$

Inequality (6) always holds for pattern 4-6 since  $\text{Sign}(\ell_\beta(s_2), \ell_j(s_1)) = 0$  only if  $j \neq \beta$  (since  $Wf(\ell_\beta(s), s) < 0$  and  $Wf(\ell_j(s), s) > 0$ ,  $j = 0, 1$ ). We will therefore focus the analysis on the inequalities (4) and (5).

For pattern 3,4,6 the decision-function successfully connects any two mod-max if *both* inequalities (4) and (5) hold for *all* scales such that  $\ell_0$  exists. Consequently (4) has to hold for every  $0 < s_1 < s^*$  and (5) for all  $0 < s_2 < s^*$ . For pattern 5 *both* (4) and (5) have to hold for *all* scales such that  $\ell_1$  is well-defined. Thus (4) has to hold for every  $0 < s_2 < s^*$  and (5) for all  $0 < s_1 < s^*$ .

**Comment:** *The preceding analysis of the decision-function  $P(\cdot, \cdot)$  focuses on patterns with values of  $A, B, \beta$  typical for our specific application (locally model medical ultrasound signals). Values of  $A, B$  and/or  $\beta$  near the 'transformation-limit' (value of  $A, B, \beta$  where a pattern transforms into another) will not be studied. In practice one can often consider such 'critical' configurations by another pattern.*

*Pattern 3:* First we consider the decision-function and corresponding time-scale filtering procedure with respect to *pattern 3*. Numerical analysis suggests that the time-scale filtering procedure is most likely to fail at the largest scale where both  $\ell_1$  and  $\ell_0$  exist. We can therefore simplify the analysis by considering the left-hand-side (lhs.) of (4) with  $s_1 = s^*$ ,  $s_2 = 2s_1$  and lhs. of (5) with  $s_2 = s^*$ ,  $s_1 = s_2/2$ . Note that the lhs. of (4) and (5) - denoted  $Q_1(A)$  and  $Q_0(A)$  - are now functions depending *only* on  $A$ . In particular, if both  $Q_1(A) > 0$  and  $Q_0(A) > 0$  the suggested procedure holds.

Fig.4 displays the graphs of respectively  $Q_1(A)$  and  $Q_0(A)$  for  $P(\cdot, \cdot)$  given by (1) with control-parameters  $\alpha = \{-1/2, 0, 1/2, 1, 3/2\}$  (cyan, yellow, blue, red, green). The dashed and dash-dotted lines correspond to the 'limit cases' resp.  $P(n, m) = D(n, m)$  and  $P(n, m) = \Delta(n, m)$ .

From fig.4a one can see that along the maxima-line  $\ell_1$  the decay-criterion (dotted line) is optimal for connecting mod-max; if  $P(n, m) = D(n, m)$  then  $Q_1(A) > 0$  (i.e. (4) holds) for all  $A > 1$ . Along  $\ell_0$  one need to have  $A \gtrsim 1.3$ , fig.4b. On the contrary; if one considers the distance-criterion



(dash-dotted line) it suffices to have  $A > 1$  at fine scales, but needs to have  $A \gtrsim 1.3$  at coarse scales. Consequently one must have  $A \gtrsim 1.3$  in order to connect mod-max between any two scales  $s_2 = 2s_1$  and  $0 < s_1 < s^*$  for pattern 3 if either  $P(n, m) = D(n, m)$  or  $P(n, m) = \Delta(n, m)$ .

Combining distance and decay increase the  $A$ -interval for which the time-scale filtering procedure works, fig.4. If e.g.  $P(n, m)$  is given by (1) with  $\alpha = 0$  (yellow line) then it suffices to have  $A \gtrsim 1.1$  to connect mod-max between (any) two scales in pattern 3. If  $\alpha = 1/2$  (blue line) then both  $Q_1(A) > 0$  and  $Q_0(A) > 0$  for all  $A \gtrsim 1.16$ .

*Pattern 4:* For *pattern 4* there are three maxima-lines,  $\ell_0$ ,  $\ell_1$  and  $\ell_\beta$ . As illustrated in

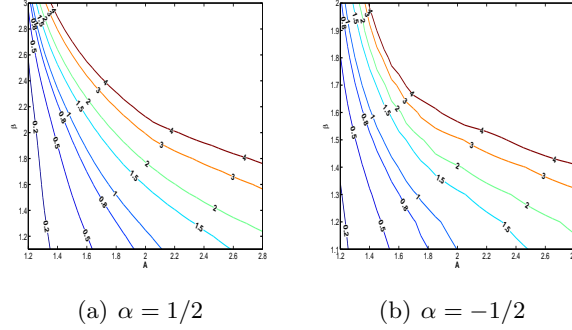


Figure 5: Numerical analysis of  $Q_1$  for pattern 4. The figures display level curves of the surface  $Q_1(A, B, \beta) = 0$  for  $P(n, m)$  given by (1) with (a)  $\alpha = 1/2$  and (b)  $\alpha = -1/2$ . NOTE that in (a) we consider  $1.1 < \beta < 3$  and in (b)  $1.1 < \beta < 2$ .

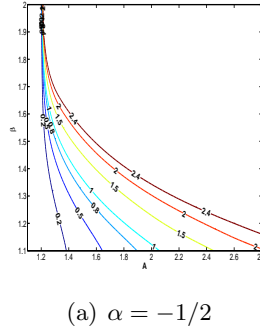


Figure 6: Numerical analysis of  $Q_0$  for pattern 4. The figure displays some level-curves of the surface  $Q_0(A, B, \beta) = 0$  for  $P(n, m)$  given by (1) with  $\alpha = -1/2$ .

fig.3h the edge at  $\beta$  'repels' the maxima-lines corresponding to the edges at 0 and 1. The result is that the distance between  $\ell_0$  and  $\ell_1$  gets smaller, hence weakening the distance-criterion for pattern 4.

For pattern 4 the time-scale filtering procedure successfully connect mod-max across scales if both (4) and (5) holds. For this purpose let  $Q_1(A, B, \beta)$  denote the minimum of the lhs. of (4) with respect to  $s_2 = 2s_1$ ,  $0 < s_1 < s^*$ ,  $j = 0$  and  $0 < B < B^*$ , where  $B^*$  is given by (2) (recall that pattern 4 transforms into pattern 5 for  $B > B^*$ ). Similarly let  $Q_0(A, B, \beta)$  denote the minimum of the lhs. of (5) with  $s_1 = 2s_2$ ,  $0 < s_2 < s^*$ ,  $j = 1$  and  $0 < B < B^*$ . If both  $Q_1(A, B, \beta) > 0$  and  $Q_0(A, B, \beta) > 0$  the procedure successfully connects any two mod-max with respect to pattern 4.

The additional variables  $B$  and  $\beta$  make the analysis of  $Q_1$  and  $Q_0$  more complicated for pattern 4-6 than for pattern 3. Rather than considering the graphs of  $Q_1$  and  $Q_0$  we study the (level-curves of the) surfaces  $Q_i(A, B, \beta) = 0$ ,  $i = 0, 1$ . Numerical analysis indicates that both  $Q_1$  and  $Q_0$  increase if: (i): the jump at location 1 increases, (ii): the jump at  $\beta$  decreases, or (iii): the distance from

1 to  $\beta$  increases. In particular, if  $Q_1(A_0, B_0, \beta_0) = 0$  then  $Q_1(A, B, \beta) > 0$  for all  $A > A_0, B_0 > B > 0$  and  $\beta > \beta_0$ , and similarly for  $Q_0$ .

As with pattern 3; different values of the control-parameter  $\alpha$  'interpolates'  $P(\cdot, \cdot)$  given by (1) in between the 'limit' cases  $P(n, m) = D(n, m)$  and  $P(n, m) = \Delta(n, m)$ . Fig.5 displays the level-curves of the surface  $Q_1(A, B, \beta) = 0$  with respect to  $P(n, m)$  given by (1) with  $\alpha = \pm 1/2$  (note that the y-axis differs in the figures). Fig.6 displays the level-curves of  $Q_0(A, B, \beta) = 0$  for  $\alpha = -1/2$ . Numerical studies indicate that  $Q_0(A, B, \beta) > 0$  if  $\alpha = 1/2$ , except possibly near critical values of  $A, B, \beta$  such as e.g.  $\beta \approx 1$  (which are uninteresting to study for our purpose).

As expected; increasing the influence of the decay-criterion increases the accuracy of the time-scale filtering procedure for pattern 4. The following table illustrates this for a few concrete values of  $A$  and  $\beta$ . The table shows the maximal  $B$ -interval such that the time-scale filtering procedure works for some values of  $A$  and  $\beta$ ;

A	$\beta$	$\alpha = -1/2$	$\alpha = 1/2$	$P = \Delta$
2	1.6	$0 < B < 4.57$	$0 < B < 1.52$	$0 < B < 0.83$
1.5	1.6	$0 < B < 1.35$	$0 < B < 0.54$	$0 < B < 0.25$

As one can observe in the table, the reliability of the time-scale filtering procedure increases with respect to pattern 4 if we increase the influence of the decay-criterion.

*Pattern 5:* For *pattern 5* the situation is similar as with pattern 4. The edge at  $\beta$  will - as

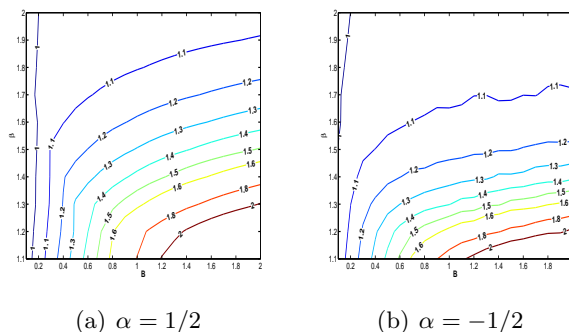


Figure 7: Numerical analysis of  $Q_0$  for pattern 5. The figures display level curves of the surface  $Q_0(A, B, \beta) = 0$  for  $P(n, m)$  given by (1) with (a)  $\alpha = 1/2$  and (b)  $\alpha = -1/2$ .

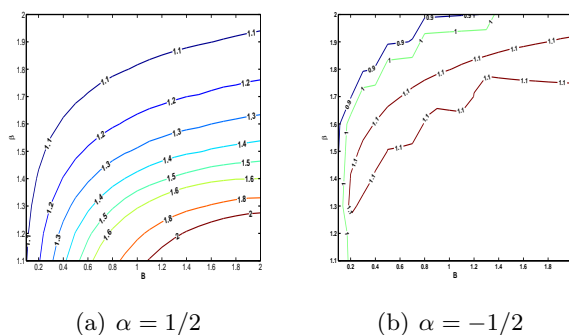


Figure 8: Numerical analysis of  $Q_1$  for pattern 5. The figures display level curves of the surface  $Q_1(A, B, \beta) = 0$  for  $P(n, m)$  given by (1) with (a)  $\alpha = 1/2$  and (b)  $\alpha = -1/2$ .

before - 'push' the other maxima-lines away. However, since the 'long' maxima-line now approaches 0 (and not 1 as for pattern 4, fig.3(h,j)), we expect that the distance-criterion will be strengthened.

Let as before  $Q_1(A, B, \beta)$  denote the minimum of the lhs. of (4) for  $0 < s_2 < s^*$ ,  $s_2 = 2s_1$ ,  $j = 0$  and  $0 < A < A^*$ . Given  $B, \beta$  one can find  $A^*$  by solving (2). Let  $Q_0(A, B, \beta)$  denote the minimum of the lhs. of (5) for  $0 < s_1 < s^*$ ,  $s_2 = 2s_1$ ,  $j = 1$  and  $0 < A < A^*$ .

Fig.7 and fig.8 show some level-curves of the surfaces  $Q_i(A, B, \beta) = 0$ ,  $i = 0, 1$  for  $P(n, m)$  defined in (1) with  $\alpha = \pm 1/2$ . Given the pair  $(B, \beta)$  in the  $B\beta$ -plane the point  $(B, \beta, A)$  on the surface  $Q_i(A, B, \beta) = 0$  represents the maximal value of  $A$  such that the procedure successfully connects mod-max along the maxima-line  $\ell_i$  for  $i = 0, 1$ .

One may observe that the reliability of the decision function  $P(\cdot, \cdot)$  increases if we increase the weighting of the distance-criterion. Indeed;  $Q_i(A, B, \beta) > 0$ ,  $i = 0, 1$  for 'almost' all  $0 < A < A^*$  if  $P(n, m) = \Delta(n, m)$  or if  $P(n, m)$  is given by (1) with  $\alpha = 1/2$ . On the other hand, if  $\alpha = -1/2$  one can roughly say that one must have  $A \lesssim 1$  to ensure that both  $Q_1 > 0$  and  $Q_0 > 0$ .

*Pattern 6:* Fig.9 and fig.10 show a few examples of the analysis of the decision-function with respect to *pattern 6*. Similar to the previous patterns let  $Q_1(A, B, \beta)$  denote the minimum of the lhs. of (4) wrt.  $s_2 = 2s_1$ ,  $0 < s_1 < s^*$ ,  $j = 0$  and  $A > A^*$ . Given  $(B, \beta)$  one can find  $A^*$  by solving (2) (If  $A = A^*$  the maxima-line at coarse scales trifurcates). Let  $Q_0(A, B, \beta)$  denote the minimum of the lhs. of (5) wrt.  $s_2 = 2s_1$ ,  $0 < s_2 < s^*$ ,  $j = 1$  and  $A > A^*$ .

Fig.9 and fig.10 show some results of the analysis of pattern 6 with  $B = kA$  for  $0 < k < 1$  and  $0.1 < \beta < 0.9$ . If  $\beta$  is close to either 0 or 1 one can in practice model the signal as pattern 1, pattern 2 or pattern 3, depending on mutual relations between  $k$  and  $\beta$ . For large values of  $\beta$  and  $k > 1$  the maxima-lines become unstable making numerical analysis difficult.

The surfaces  $Q_i(A, B, \beta) = 0$ ,  $i = 0, 1$  represent the minimal  $A_0 > 0$  such that  $Q_i(A, B, \beta) > 0$  for all  $A > 0$ . Fig.9 shows some level-curves of the surface  $Q_1(A, B, \beta) = 0$  for  $P(n, m)$  given by (1) with  $\alpha = \pm 1/2$ . Fig.10 shows the some level-curves of the surface  $Q_0(A, B, \beta) = 0$  for  $P(n, m)$  given by (1) with  $\alpha = -1/2$ . Numerical studies suggest that  $Q_0(A, B, \beta) > 0$  for all  $0.1 < \beta < 0.9$ ,  $0 < B < A$  and  $A^* < A$  if  $\alpha = 1/2$  or  $P = \Delta$ , except possibly for  $A \approx A^*$ .

One may observe in fig.9 and fig.10 that increasing the influence of the distance-criterion increases the reliability of the scale-space filtering procedure for pattern 6. This is caused by the edge at  $0 < \beta < 1$  which 'pushes' the other maxima-lines away in different directions and hence strengthens the distance-criterion. In addition, the edge at  $\beta$  has negative intensity  $B$  which disrupts the decay-coefficient of the wavelet transform, and hence the accuracy of the decay-criterion.

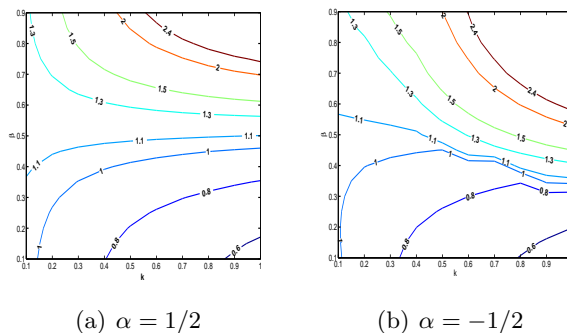


Figure 9: Numerical analysis of  $Q_1$  for pattern 6. The figures display level curves of the surface  $Q_1(A, B, \beta) = 0$  for  $P(n, m)$  given by (1) with (a)  $\alpha = 1/2$  and (b)  $\alpha = -1/2$ .

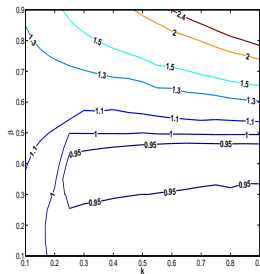
(a)  $\alpha = -1/2$ 

Figure 10: Numerical analysis of  $Q_0$  for pattern 6. The figure display level curves of the surface  $Q_0(A, B, \beta) = 0$  for  $P(n, m)$  given by (1) with  $\alpha = -1/2$ .

### 3.4 Summary and discussion of 1-D time-scale filtering procedure.

We have studied the suggested time-scale filtering procedure from Sect.3.1 with respect to the six model-patterns in Sect.3.2.

Connecting mod-max across time-scale plane for the first two patterns is trivial. For the other patterns the overall accuracy of the decision-function  $P(\cdot, \cdot)$  in general increases if we use a suitable weighting between the distance- and decay-criterion. For pattern 3 and pattern 4 the accuracy of the decision-function  $P(\cdot, \cdot)$  benefits from increasing the influence of the decay-criterion. For the last two patterns we saw that increasing the influence of the distance-criterion increases the accuracy of the time-scale filtering procedure. It is clear that one should take specific features of the concrete signals into account when defining the mutual weighting between distance- and decay-criterion. When analyzing the medical ultrasound images in Sect.5.3 we use  $\alpha=0$ .

In Sect.5.1 we will evaluate the performance of the proposed time-scale filtering procedure with respect to medical ultrasound signals.

The results from the previous sections are useful also for more complicated signals. For instance the signal  $f(t) = \rho(t) + A\rho(t-1) + B'\rho(t-7) - A'\rho(t-9) + \rho(t-10)$  is locally similar to pattern 3 near the point 0 and pattern 4 near the point 10. Due to fast decay of the wavelet  $\psi_s(t)$  the maxima-lines of the 'local' patterns in  $f(t)$  and their exact equivalent are practically identical for  $0 < s < 3$ . It makes little sense to analyze the signal at scales  $s > 3$  for the purpose of edge-detection. Our analysis of actual medical ultrasound signals indicates that such signals often are composed of (distinct) patterns in this manner as illustrated in fig.2.

Real medical ultrasound signals are of course 'smooth'. The corresponding edges can be modeled by smoothed versions of the 'ideal' patterns in Sect.3.2. If  $f$  is any of the ideal patterns say, then we can model the smoothed patterns as  $h = f * g_\sigma$  where  $g_\sigma(t) = \frac{1}{\sqrt{2\pi\sigma}} e^{-t^2/2\sigma^2}$ ,  $\sigma > 0$ , is the Gaussian smoothing kernel.

With some natural modifications the suggested time-scale filtering procedure applies to the smoothed patterns as well. We need to use denser (i.e. non-dyadic) scales; more precisely we need to choose  $s_2, s_1$  such that  $\sqrt{s_2^2 + \sigma^2} = 2\sqrt{s_1^2 + \sigma^2}$ . If we in addition change  $\dots - 1/2$  to  $\dots - 1/2 - \frac{\ln \frac{s_2}{2s_1}}{\ln 2}$  in the expression for the decay-criterion  $D(n, m)$ , the results from Sect.3.3 apply directly (i.e. with the same  $A, B, \beta$ ).

### 3.5 Decision-function and space-scale filtering procedure for 2-D signals.

We turn the attention towards a space-scale filtering procedure for connecting mod-max across the *space-scale plane* of 2-D signals. In images mod-max are chained together to form *boundary-curves* corresponding to boundaries of objects, and the natural space-scale plane object is the *maxima-surface*. The behavior of a maxima-surface is more subtle than for a maxima-line. For instance one can not assume that a maxima-surface does not branch. The target with the space-scale filtering procedure is to decide which mod-max propagate toward each of the boundary-curves at the finest scale.

The suggested decision-function for 2-D signals is - with some natural modifications - similar to the 1-D decision-function defined in Sect.3.1. Let  $s_2$  and  $s_1$  be two scales  $s_2 > s_1$ , and let  $(n, s_2) = ((n_1, n_2), s_2)$  and  $(m, s_1) = ((m_1, m_2), s_1)$  be two mod-max. We define the decision-function as;

$$P(n, m) = \Delta(n, m)D(n, m)\text{Angle}(n, m)$$

where;

$$\begin{aligned} \Delta(n, m) &= \exp(-|n - m|s_1^{-\alpha}) \\ D(n, m) &= \exp\left(-\left|\ln \frac{|Wf(n, s_2)|}{|Wf(m, s_1)|} \ln^{-1} \frac{s_2}{s_1} - 1\right|s_1^\alpha\right) \\ \text{Angle}(n, m) &= \exp(-|Af(n, s_2) - Af(m, s_1)|). \end{aligned}$$

$Af(u, s)$  is the direction of the wavelet transform at the mod-max  $(u, s)$ , and is given by

$$Af(u, s) = \begin{cases} \arctan \frac{Wf^y(u, s)}{Wf^x(u, s)} & Wf^x(u, s) \geq 0 \\ \pi + \arctan \frac{Wf^y(u, s)}{Wf^x(u, s)} & Wf^x(u, s) < 0. \end{cases}$$

The essence of the space-scale filtering procedure is - as in 1-D - to connect mod-max which maximize  $P(n, m)$ .

In particular, if one consider 2-D patterns obtained by a tensor product of the 1-D patterns, then the analysis in Sect.3.3 extends to the 2-D procedure.

Given two scales  $s_2 > s_1$  the procedure requires that for each  $n \in \mathcal{M}f(s_2)$  one has to compute  $P(n, m)$  for every  $m \in \mathcal{M}f(s_1)$ . One can reduce the computational efforts by computing  $P(n, m)$  only for  $m \in \mathcal{M}f(s_1)$  within a given distance ( $4s_1$  should suffice if we use dyadic scales) of  $n$ .

In the next section we will see that for our purpose it is sufficient to compute  $P(n, m)$  for only a few mod-max at scale  $s_2$  as well. By using these simplification one will effectively reduce the computational complexity of the space-scale filtering procedure for images.

## 4 Edge-detection.

The uncertainty-principle states that in a noisy signal there exists no single scale such that one can detect and simultaneously localize only the significant edges, [3]. However, by using the maxima-lines one can turn the uncertainty-principle into our advantage. At coarse scale one can detect the significant edges in the signal, and at fine scales one can localize them. Since maxima-lines connect coarse- and fine-scale information one can effectively improve edge-detection in noisy signals.

In this section we discuss a multi-scale wavelet-based edge-detection scheme. The method is based on the suggested time-scale filtering procedure and a perceptual criteria similar to that in [6]. This approach has shown promising results for detecting and localizing (low-contrast) edges in medical images.

### 4.1 1-D edge-detection.

Assume that the wavelet transform is computed at scales  $s_j$  for  $j = 1, \dots, J$ , and let  $\mathcal{M}f(s_1)$  denote the mod-max at the finest scale  $s_1$ . For a mod-max  $a \in \mathcal{M}f(s_1)$  let  $\ell_a$  denote the maxima-line which contains  $a$ . To each  $a$  assign the number;

$$R(a) = \sum_{(u,s) \in \ell_a} |Wf(u, s)|.$$

If need be one can introduce a weight-function  $\mu(s)$  in the expression for  $R(a)$ , for instance to favor fine/coarse scale information. The final step of the edge-detector is to decide a threshold  $T > 0$  and find the mod-max  $a \in \mathcal{M}f(s_1)$  such that  $R(a) > T$ . These mod-max are used to represent the significant edges in the signal.

### 4.2 2-D edge-detection

Assume that the wavelet transform is computed at scales  $s_j$  for  $j = 1, \dots, J$  and let  $c_j$  denote the boundary-curves at scale  $s_1$ .

To each maxima-curve  $c_j$  we assign the following quantity;

$$S(c_j) = (\text{length of } c_j) \cdot \text{av}(\{R(a) : a \in c_j\}), \quad (7)$$

where  $\text{av}(\cdot)$  denotes the average-function. The final step of the edge-detection is to identify the curves  $c_j$  such that  $S(c_j) > T$ , where  $T > 0$  is a threshold. These boundary-curves is used to represent the boundaries of significant edges in the image.

The quantity  $\text{av}(\{R(a) : a \in c_j\})$  reduces the influence of a few false connections made by the space-scale filtering procedure along a boundary-curve  $c_j$ . Such false connections can occur for some 'critical' patterns (e.g.  $A \approx 1$  in pattern 3).

As mentioned in Sect.3.5 one can save computational efforts by reducing the number of  $m$ 's for which one has to compute  $P(n, m)$ . Further reduction can be achieved by computing the average in (7) from only a 'few' randomly selected maxima-lines from each maxima-curve  $c_j$ . Experiments indicate that this simplification has little influence on the values of  $S(c_j)$ .

## 5 Experiments and results.

We test the edge-detector on both phantom and actual medical ultrasound signals. By studying the algorithm on phantom-signals we compare the Figure of Merit [19] with the Canny edge-detector. The visual performance of the edge-detector is analyzed with respect to medical ultrasound signals. This analysis focuses on some well-known problem features of medical ultrasound images; such as low-contrast edges and speckle-noise.

Before studying the edge-detection algorithm we analyze the reliability of the suggested time-scale filtering procedure on actual signals. The main question is whether the results from Sect.3 also apply to actual medical ultrasound signals.

### 5.1 Accuracy of time-scale filtering procedure on medical ultrasound signals.

To quantitatively evaluate the performance of the suggested time-scale filtering procedure from Sect.3.1 we compare the output of the procedure with the exact maxima-lines of the wavelet transform. Assuming that the procedure connects the mod-max  $(n, s_2)$  to  $(m, s_1)$  and  $n = \ell_a(s_2)$  say, then we will study if  $m = \ell_a(s_1)$ . The test-signals used to evaluate the procedure are 1-D cross-sections

of medical ultrasound images.

In the analysis we study the probability of a false connection, and between which scales an error is most likely to occur. For the purpose of edge-detection the severity of a false connection increases at coarse scales. We also study the average displacement (in pixels) of a mod-max caused by a false connection. If this number is small it indicates that an error has little influence on the visual output of the edge-detector.

In the experiments we use scales  $s = 2^j$ ,  $1 \leq j \leq 5$ . The control-parameter is chosen as  $\alpha = \{-1/2, 0, 1/2\}^1$ . To obtain the actual maxima-lines we use the edge-focusing algorithm [4].

The results of the quantitative analysis of the time-scale filtering procedure is displayed in Tab.1-3. Each column represents the average performance of the procedure applied to every horizontal cross-section in the corresponding image. The images are displayed in fig.12(a,b,c) and fig.11b.

The analysis of pattern 6 in Sect.3.3 showed that the accuracy of the suggested time-scale

<b>Signal:</b>	Tumor	Blood - vessel	Liver	phantom
False connections (%):	4.8	4.7	6.2	4.2
Spatial error in pixels:	12.4 (2.5)	12.9 (2.5)	12.2 (2.8)	20.3 (7.4)
False connections between scale 32 and 16:	2.5	4.4	8.5	4.2
False connections between scale 16 and 8:	5.4	5.2	9.0	8.0
False connections between scale 8 and 4:	6.2	5.7	8.2	5.0
False connections between scale 4 and 2:	4.8	4.5	6.0	1.7

Table 1: Analysis of the time-scale filtering procedure in Sect.3.1 on medical ultrasound signals. The control-parameter between distance- and decay-criteria is  $\alpha=1/2$ . The number in parenthesis on the 2. row is the spatial error in percent relative to size of the signal.

<b>Signal:</b>	Tumor	Blood - vessel	Liver	phantom
False connections (%):	4.0	4.2	4.8	3.8
Spatial error in pixels:	11.5 (2.2)	13.2 (2.6)	12.6 (2.9)	19.2 (7.0)
False connections between scale 32 and 16:	1.9	4.3	8.6	3.3
False connections between scale 16 and 8:	4.3	5.3	7.9	8.0
False connections between scale 8 and 4:	5.2	4.8	5.4	4.1
False connections between scale 4 and 2:	4.1	3.9	4.7	1.6

Table 2: Analysis of the time-scale filtering procedure in Sect.3.1 with control-parameter  $\alpha=0$ .

filtering procedure increases as  $\alpha$  increases from  $-1/2$  to  $1/2$ . Speckle noise can often locally be modeled as pattern 6 (with  $A \approx B \approx 1$  and  $\beta \approx \frac{1}{2}$ ). Hence we expect to observe a similar increase in accuracy for actual medical ultrasound signals. In Tab.1-3 one can indeed observe such increase

<sup>1</sup>Note that in the analysis of the patterns in Sect.3 we had  $s_1 < 1$  in the expression for  $P(n, m)$  in (1). In particular  $s_1^{1/2} < s_1^0 < s_1^{-1/2}$ . Since we are using scales  $s = 2^j$ ,  $1 \leq j \leq 5$  to analyze actual medical ultrasound signals we will necessarily have  $s_1^{1/2} > s_1^0 > s_1^{-1/2}$ . This causes that a large  $\alpha$  favors decay-criteria and a small favors the distance-criteria. I.e.  $\alpha = -1/2$  in the preceding section 'corresponds' to  $\alpha = 1/2$  in this section, and visa verse for  $\alpha=1/2$ .

<b>Signal:</b>	Tumor	Blood - vessel	Liver	phantom
False connections (%):	3.9	4.0	4.6	3.7
Spatial error in pixels:	11.7 (2.3)	13.5 (2.6)	13.3 (3.1)	19.3 (7.0)
False connections between scale 32 and 16:	1.9	4.3	8.6	3.3
False connections between scale 16 and 8:	4.4	5.3	7.8	7.8
False connections between scale 8 and 4:	5.0	4.5	5.2	4.0
False connections between scale 4 and 2:	4.0	3.7	4.5	1.6

Table 3: Analysis of the time-scale filtering procedure in Sect.3.1 with control-parameter  $\alpha = -1/2$ .

of the accuracy of the procedure on medical ultrasound signals (recall that  $\alpha=1/2$  in this analysis corresponds to  $\alpha = -1/2$  in the analysis in Sect.3, etc). A closer inspection indicates that false connections *in between* maxima-lines corresponding to speckle-noise is the typical problem for the time-scale filtering procedure on ultrasound signal. Since speckle-noise contains information which is unwanted from an edge-detection viewpoint, such false connections will only be a minor problem.

## 5.2 Results of edge-detection on phantom ultrasound images.

To study the performance of the edge-detection algorithm suggested in Sect.4.2 we compare it with the well-known Canny edge-detector. We believe that comparing the Canny edge-detector with ours demonstrates some differences between multi-scale and single-scale wavelet-based edge-detection.

For the Canny edge-detector with hysteresis we have used thresholds  $T_{\text{low}} = 0.1 \cdot \max |Wf((\cdot, \cdot), s)|$  and  $T_{\text{high}} = 0.3 \cdot \max |Wf((\cdot, \cdot), s)|$ . The scale is chosen equal to the finest scale used by our algorithm.

To quantitatively analyze the edge-detectors we study the phantom medical ultrasound signals shown in fig.11. The image in fig.11(a) shows the noise-free version, and fig.11(b,c) shows the

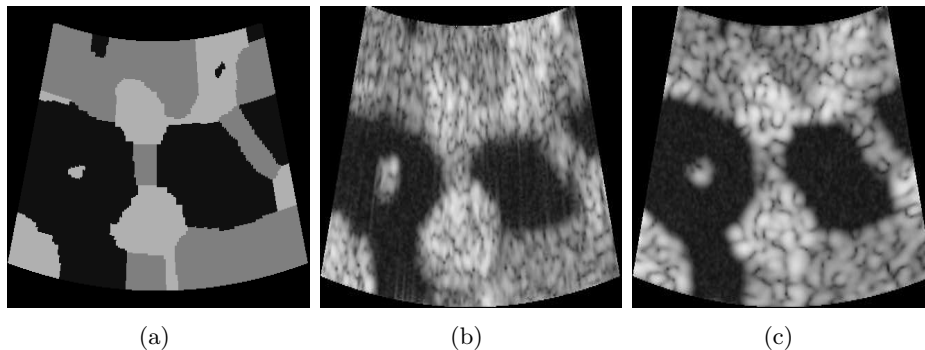


Figure 11: Phantom medical ultrasound images. (a) Noise-free image, (b,c) images with speckle-noise.

images with various speckle-noise. The phantom images are generated by using a region image as a variance field for the diffuse scattering. The images are made by convolving the ideal image with a parametric point-spread function and adding white Gaussian noise, and are discussed in details in [20, 21]<sup>2</sup>.

<sup>2</sup>The images are kindly provided by SINTEF MedTech. The author thanks T. Langø for his assistance.



Signal:	proposed edge-detector	Canny
phantom 1:	0.56	0.53
phantom 2:	0.54	0.47

Table 4: The Figure of Merit of the edge-detection algorithm in Sect.4.2 and the Canny edge-detector at scale 4.

Signal:	proposed edge-detector	Canny
phantom 1:	0.54	0.53
phantom 2:	0.53	0.51

Table 5: The Figure of Merit of the edge-detection algorithm in Sect.4.2 and the Canny edge-detector at scale 6.

We use the well-known Figure of Merit (FOM)[19] to quantitatively evaluate the edge-detection algorithms. The FOM is the number defined as;

$$\text{FOM} = \frac{1}{\max\{n_p, n_d\}} \sum_1^{n_d} \frac{1}{1 + \gamma d_i^2},$$

where  $n_p$  and  $n_d$  are the number of resp. true and detected edges, and  $d_i$  is the minimal distance from a detected to a true edge.  $\gamma$  is a constant used to penalize displaced mod-max. To be consistent with others we use  $\gamma=0.11$  [8, 22]. The FOM should ideally be close to 1.

The values of the Figure of Merit of the two edge-detectors are displayed in tab.4-5.

### 5.3 Result of edge-detection on real ultrasound images.

In this section we discuss the results of the suggested edge-detection algorithm on real signals. For this purpose we study the edges detected by the algorithm in several actual medical ultrasound images. The goal is to study if the algorithm detects the significant edges in the images without including irrelevant information such as noise. In addition we discuss how one can obtain a threshold as well as the computational complexity of the algorithm.

Fig.12 shows the ultrasound images which are discussed in this section. Each image contains

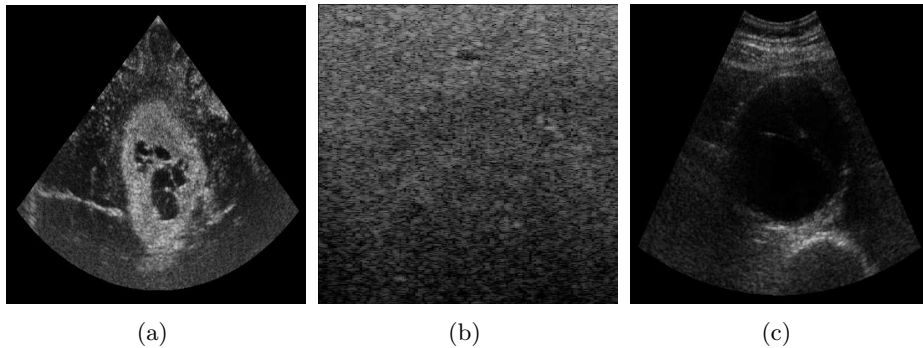


Figure 12: (a) : Tumor-image, (b) : Liver-image, (c) : Blood-vessel image.

some typical features of medical ultrasound images which cause difficulties for edge-detection.

*Fig.12(a), Brain-tumor image:* The interesting edges are the outer boundary of the tumor and the cortex (white 'horizontal' object to the south-west of the tumor). The voids within the tumor are mainly interesting in order to study how the edge-detector represents fine details.

*Fig.12(b), Liver image:* The interesting edge is the boundary of the liver. The boundary is the horizontal line in the upper third in the image. This image interesting to study because of the low CNR of the boundary.

*Fig.12(c), Blood-vessel image:* In this image we want to detect the boundary of the blood-vessel. Some parts of the boundary of the blood-vessel have low contrast making them difficult to detect. This problem is typical for ultrasound images of blood-vessels.

*Edge-detection and noise-removal:* Fig.13(a,b,c) shows some results of our edge-detection

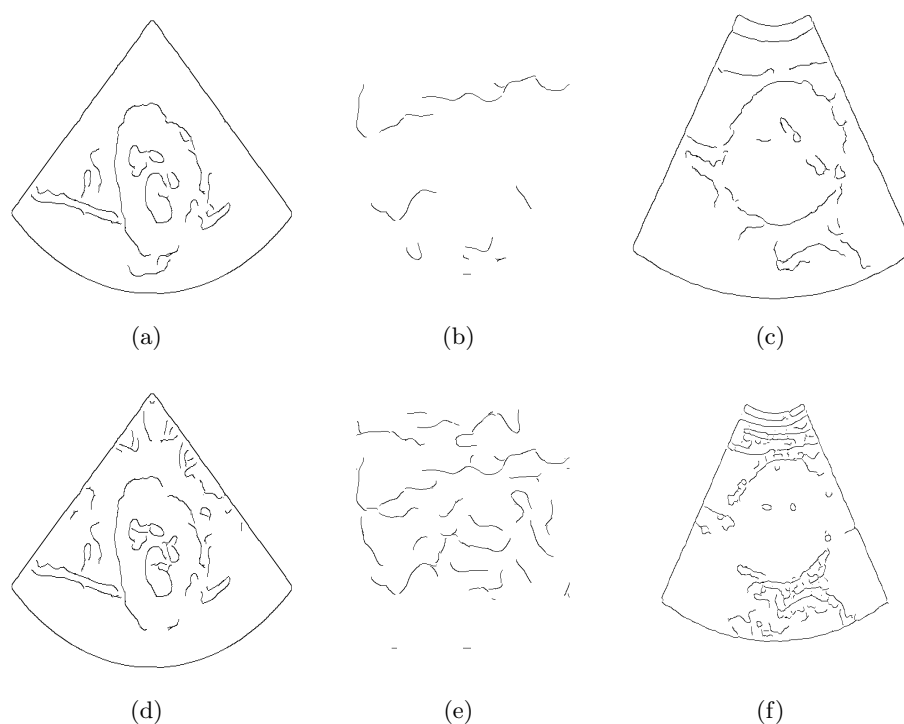


Figure 13: Results of the edge-detection algorithm of the images in fig.12. In figure (a) - (c) we display the results of the edge-detection algorithm studied in Sect.4 . In figure (d)-(f) we display the results obtained with a Canny edge-detector. (a,d) : Tumor image, (b,e) : Liver image, (c,f) : Blood-vessel image.

algorithm applied to the images in fig.12. Most of the significant edges which we would like to detect are present in the representations. One may also observe, in particular in fig.13(a,c), that the representations contain few edges which can be ascribed to noise. The representations in fig.13 show promising results for detecting low contrast edges and fine detail edges. However, the boundary-curves of such edges are vulnerable to fragmenting (which make them difficult to detect). This phenomenon occurs for instance underneath the tumor (low contrast) and to some degree inside the tumor (fine details). The fragmenting - in particular for low-contrast edges - appears to increase due to speckle-noise. One can reduce this problem by connecting fragmented boundary-curves (e.g. by using coarse scale information as suggested in [6]). Preliminary studies have shown that using this as a complimentary tool improves edge-detection of low-contrast and fine detail edges. We use no synthesizing of the boundary-curves in this study.

Fig.13(d,e,f) shows the result obtained by using the Canny edge-detector (with hystera). The scales is chosen equal the finest scale used by our algorithm. One can observe that the edge-detector scheme studied in Sect.4.2 in general yields better representations of the significant edges in the images, and includes less noise.

*Threshold:* The edge-detector assigns to each boundary-curve  $c_j$  a value  $S(c_j)$  representing both its length and value of wavelet transform in both time- and scale-space. Values of  $S$  corresponding to noise will therefore be concentrated at low values, while those corresponding to edges will be distributed discretely at high values. The result is that there is often a separation between values of  $S$  corresponding to noise and edges. A similar phenomenon was observed in [6]. In addition, since values of  $S$  corresponding to significant edges are often distributed discretely it is possible to find representations which are perceptually optimal.

*Computational complexity:* The computational complexity of the edge-filtering procedure in Sect.4.2 is negligible. In what follows we focus on the computational complexity of computing the wavelet transform and the space-scale filtering procedure from Sect.3.5.

To reduce the computational complexity of the space-scale filtering procedure we use the tricks discussed in Sect.3.5 and Sect.4.2. In other words we find the maxima-lines of only a few randomly selected mod-max along each boundary-curve, and use a sliding window (of size  $4 \cdot \text{scale} \times 4 \cdot \text{scale}$ ) to decide candidate connections at the next finer scale. We use the fast Fourier-transform to compute the wavelet transform.

The space-scale filtering procedure has been implemented in MATLAB version 7.9.0 (R2009b) on a laptop with a Pentium 3 (2 GHz) processor. Tested on a  $362 \times 512$  image the total processing time is 4.6 seconds if we find the maxima-lines of 50% of the mod-max. If we find only 10% randomly selected maxima-lines the total processing time is 1.9 sec.

Computationally both computing the wavelet transform at different scales and connecting mod-max across scales is well-suited for parallel-computing. It is expected that this should allow us to further reduce the total processing-time of the scale-space filtering procedure.

## 6 Conclusion

We suggest a fast multi-scale edge-detection algorithm for medical ultrasound signals. The edge-detector is based on the continuous wavelet transform, and takes advantage of the behavior of maxima-lines in the space-scale plane. Our algorithm shows promising results for detecting the significant edges in medical ultrasound signals.

The key-point of the edge-detection scheme is a fast space-scale filtering procedure for medical ultrasound signals. The procedure is designed to accommodate a set of patterns modeling intensity-changes which are typical in such signals. This allow us to manage and reduce the ambiguity introduced when using the multi-scale wavelet transform to detect edges in a medical ultrasound signal. The space-scale filtering procedure connects mod-max which belong to the same maxima-line by computing the wavelet transform at only a sparse set of scales. For our medical ultrasound signals we typically need to compute the wavelet transform at the four scales  $s = \{4, 8, 16, 32\}$ . In the popular Edge-focusing algorithm [4] one computes the wavelet transform at a linear set of scales ( $\Delta s = 1/2$ ) to trace mod-max in the space-scale plane. Our proposed space-scale filtering procedure will therefore considerably reduce the computational efforts needed to decide which mod-max belong to the same maxima-line.

Based on the space-scale filtering procedure we study a novel edge-detection algorithm for medical ultrasound signals. The edge-detector assigns to each candidate edge a value representing the behavior of its corresponding maxima-line in the space-scale plane. Experimental results indicate

that the edge-detector finds both high- and low-contrast edges in medical ultrasound images and yet disregards noise. Compared to the Canny edge-detector we observe that our algorithm finds the significant edges, and includes less redundant information such as noise. Our study has showed that one can construct multi-scale edge-detection algorithm for medical ultrasound signals which meets the demand of speed, but not on the expense of reliability.

We also expect that using multi-scale information opens new possibilities for further improvements of edge-detection in medical ultrasound images. One possibility is to dynamically choose the finest scale based on local automatic scale selection as described in e.g. [16].

## Acknowledgment

The author would first of all like to thank his supervisor Prof. Yurii Lyubarskii for the support and guidance during the work.

The author would also like to thank Dr. Jianhua Yao (National Institute of Health) for useful discussions.

The author would like to thank SINTEF Medical Technology for providing medical ultrasound images obtained through clinical studies at St. Olavs Hospital, Trondheim, Norway.

## References

- [1] I. Daubechies, Ten lectures on wavelets, Society for Industrial and Applied Mathematics, Philadelphia, PA, USA, 1992.
- [2] S. Mallat, A wavelet tour of signal processing, 2nd Edition, Academic Press, 1998.
- [3] J. Canny, A computational approach to edge detection, IEEE transactions of pattern analysis and machine intelligence PAMI-8 (6) (1986) 679–698.
- [4] F. Bergholm, Edge focusing, IEEE transactions of pattern analysis and machine intelligence PAMI-9 (6) (1987) 726–741.
- [5] A. P. Witkin, Scale-space filtering: A new approach to multi-scale description, in: Proc. IEEE International Conference on Acoustics, Speech, and Signal Processing (ICASSP), Vol. 9, IEEE, San Diego, CA, 1984, pp. 150–153.
- [6] J. Lu, J. D. Weaver, J. Dennis M. Healy, Y. Xu, Noise reduction with a multiscale edge representation and perceptual criteria, in: in Proceedings of IEEE-SP International Symposium on Time-Frequency and TimeScale Analysis, 1992, pp. 555–558.
- [7] B. Sumengen, B. S. Manjunath, Multi-scale edge detection and image segmentation, in: European Signal Processing Conference (EUSIPCO), 2005.
- [8] Y. Yue, M. M. Croitoru, A. Bidani, J. B. Zwischenberger, J. W. Clark, Nonlinear multiscale wavelet diffusion for speckle suppression and edge enhancement in ultrasound images, IEEE transactions on medical imaging 25 (3) (2006) 297–311.
- [9] L. Zhang, P. Bao, Edge detection by scale multiplication in wavelet domain, Pattern Recogn. Lett. 23 (2002) 1771–1784.
- [10] M. Shah, A. Sood, R. Jain, Pulse and staircase edge models, Comput. Vision Graph. Image Process. 34 (1986) 321–343.

- [11] Y. Lu, R. C. Jain, Behaviour of edges in scale space, *IEEE transactions of pattern analysis and machine intelligence* 11 (4) (1989) 337–356.
- [12] C. Ducottet, T. Fournel, C. Barat, Scale-adaptive detection and local characterization of edges based on wavelet transform, *Signal Process.* 84 (2004) 2115–2137.
- [13] D. Ziou, S. Tabbone, Edge detection techniques - an overview, *International Journal of Pattern Recognition and Image Analysis* 8 (1998) 537–559.
- [14] S. Mallat, S. Zhong, Characterization of signals from multiscale edges, *IEEE transactions on pattern analysis and machine intelligence* 14 (7) (1992) 710–732.
- [15] S. Mallat, W. L. Hwang, Singularity detection and processing with wavelets, *IEEE transactions on information theory* 38 (2) (1992) 617–643.
- [16] T. Lindeberg, Edge detection and ridge detection with automatic scale selection, *International Journal of Computer Vision* 30 (2) (1998) 117–156.
- [17] F. Guo, Y. Yang, B. Chen, L. Guo, A novel multi-scale edge detection technique based on wavelet analysis with application in multiphase flows, *Powder Technology* 202 (1-3) (2010) 171–177.
- [18] R. Zhang, W. Ouyang, W.-K. Cham, Image multi-scale edge detection using 3-d hidden markov model based on the non-decimated wavelet, in: *Image Processing (ICIP), 2009 16th IEEE International Conference on*, 2009, pp. 2173 –2176.
- [19] W. K. Pratt, *Digital image processing*, 2nd Edition, John Wiley & Sons, Inc., 1991.
- [20] O. Husby, T. Lie, T. Langø, J. Hokland, H. Rue, Bayesian 2-d deconvolution: A model for diffuse ultrasound scattering, *IEEE transactions on ultrasonics, ferroelectrics, and frequency control* 48 (1) (2001) 121–130.
- [21] T. Langø, T. Lie, O. Husby, J. Hokland, Bayesian 2-d deconvolution: Effect of using spatially invariant ultrasound point spread functions, *IEEE transactions on ultrasonics, ferroelectrics, and frequency control* 48 (1) (2001) 131–141.
- [22] S. Yi, D. Labate, G. R. Easley, H. Krim, A shearlet approach to edge analysis and detection, *IEEE Transactions on Image Processing* 18 (5) (2009) 929–941.